Cross-Track Infrared Sounder FPAA Performance

S. Masterjohn, A.I. D'Souza, L.C. Dawson, P.N. Dolan, G. Jefferson, M.G. Stapelbroek, R.W. Willis
DRS Sensors and Targeting Systems, 3400 E. Miraloma Avenue, Anaheim, CA 92806

P.S. Wijewarnasuriya*, E. Boehmer
Rockwell Scientific Company, 5212 Verdugo Way, Camarillo, CA 93012

J. Ehlert, J.E. Andrews
ITT Industries, 1919 W. Cook Rd., Ft. Wayne, IN 46818

* Presently at US Army Research Laboratory, 2800 Powder Mill Road, Adelphi, MD 20783

ABSTRACT

The Cross-track Infrared Sounder (CrIS), an interferometric sounder, is one of the instruments within the National Polar-orbiting Operational Environmental Satellite System (NPOESS) suite. CrIS measures earth radiances at high spectral resolution providing accurate and high-resolution pressure, temperature and moisture profiles of the atmosphere. These profiles are used in weather prediction models to track storms, predict levels of precipitation etc. Each CrIS instrument contains three Focal Plane Array Assemblies (FPAAs): SWIR [λ_c(98 K) ~ 5 μm], MWIR [λ_c(98 K) ~ 9 μm], and LWIR [λ_c(81 K) ~ 16 μm]. Each FPAA consists of nine large (850-μm-diameter) photovoltaic detectors arranged in a 3 x 3 pattern, with each detector having an accompanying cold preamplifier. This paper describes the selection methodology of the detectors that constitute the FPAAs and the performance of the CrIS SWIR, MWIR and LWIR proto-flight FPAAs.

The appropriate bandgap n-type $Hg_{1-x}Cd_xTe$ was grown on lattice-matched CdZnTe. 850-μm-diameter photodiodes were manufactured using a Lateral Collection Diode (LCD) architecture. Custom pre-amplifiers were designed and built to interface with these large photodiodes. The LWIR, MWIR and SWIR detectors are operated at 81 K, 98 K and 98 K respectively. These relatively high operating temperatures permit the use of passive radiators on the instrument to cool the detectors. Performance goals are D* = 5.0 x 10^{10} cm-Hz$^{1/2}$/W at 14.0 μm, 9.3 x 10^{10} cm-Hz$^{1/2}$/W at 8.0 μm and 3.0 x 10^{11} cm-Hz$^{1/2}$/W at 4.64 μm. Measured mean values for the nine photodiodes in each of the LWIR, MWIR and SWIR FPAAs are D* = 5.3 x 10^{10} cm-Hz$^{1/2}$/W at 14.0 μm, 1.0 x 10^{11} cm-Hz$^{1/2}$/W at 8.0 μm and 3.1 x 10^{11} cm-Hz$^{1/2}$/W at 4.64 μm. These compare favorably with the BLIP calculated at the nominal flux condition are D* = 8.36 x 10^{10} cm Hz$^{1/2}$/W at 14.0 μm, 1.4 x 10^{11} cm-Hz$^{1/2}$/W at 8.0 μm and 4.1 x 10^{11} cm-Hz$^{1/2}$/W at 4.64 μm.

1.0 INTRODUCTION

The Crosstrack Infrared Sounder (CrIS) is a key instrument being developed for the National Polar-Orbiting Operational Environmental Satellite System (NPOESS).[x] The CrIS instrument is a three-spectral-band Fourier Transform infrared (FTIR) spectrometer designed to measure vertical atmospheric profiles of temperature, moisture, and pressure. CrIS employs large-area detectors and requires high detector performance and linear photoresponse. Photovoltaic mercury cadmium telluride (HgCdTe) detectors coupled with the right amplifier provide both the near-theoretical background-limited infrared performance (BLIP) and the required linear response and are therefore desirable for interferometric infrared sounders such as CrIS. The CrIS instrument uses 850-μm-diameter photovoltaic detectors packaged into Focal Plane Array Assemblies (FPAAs) for the three spectral bands: SWIR, MWIR, and LWIR. Each FPAA comprises nine separate detectors arranged in a 3 x 3 pattern with an accompanying cold JFET preamplifier and associated passive electronic elements.

This paper outlines the data collected during the ProtoFlight assembly testing of all three FPAAs (SWIR, MWIR & LWIR). The focus of this paper, however, is the LWIR FPAA, the most stressing of the three colors. Each assembly is tested separately in the CrIS dedicated nitrogen heli-tran dewar. The FPAA assembly is connected to the warm electronics via a constantan cable and vacuum feedthru hermetic connector. Each FPAA has its own Circuit Card Assembly (CCA) that contains a warm amplifier and the second stage 300Hz high pass filter. One warm cable assembly provides the FPAA signals for all three bands. The CCA also provides the biases for the cold JFET pair on the cold electronics Ceramic Multilayer Board (CMLB). During some tests, the second stage coupling capacitor was defeated in order to collect DC data outputs.

2.0 PHOTODIODES

The baseline detector architecture is a p-on-n double layer planar heterostructure (DLPH) diode[1]. MBE is used to grow the appropriate bandgap n-type $Hg_{1-x}Cd_xTe$ on lattice matched CdZnTe. Wafer material is grown with wider bandgap cap layers, the subsequent detector architecture translating into the DLPH architecture. 850 μm diameter detectors are manufactured using the lateral collection diode (LCD) architecture[2] to reduce the probability of a performance degrading defect[3] intersecting the detector p/n junction.

2.1 Wafer level I-V measurements

850 μm diameter photodiodes are fabricated on a $Hg_{1-x}Cd_xTe$ wafer laid out on a grid that permits dicing the wafer into single photodiodes each of which are 2 mm x 2 mm. At the top and running through the middle of the wafer are process evaluation chips (PECs). Variable area photodiodes incorporated into the PECs provide the first optical evaluation of the $Hg_{1-x}Cd_xTe$ layers quantum efficiency and cutoff wavelength. The processed wafer is diced into half to provide access to the PECs running through the center of the wafer. Each half wafer is inserted into 100 pin socket carriers permitting bonding to every photodiode. A drawing of the half wafer is shown in Figure 1. Each half wafer contains 78 photodiodes. I-V curves between –200 mV and +100 mV are obtained for every photodiode on the wafer. This is the preliminary screen that selects photodiodes that will be inserted into 68 pin leadless chip carriers for further measurements that include quantum efficiency, spectral response, confirmation of the I-V characteristics, and noise measured in a dark and illuminated environment. Figure 2 is a plot of the I-V curves at 81 K for 78 LWIR photodiodes. Photodiodes with dark currents less than 72 μA at 60 mV reverse bias, the LWIR photodiodes operating voltage, are selected for QE and noise measurements. Similar I-V measurements albeit with different screening criteria are made at 98 K for MWIR and SWIR photodiodes.

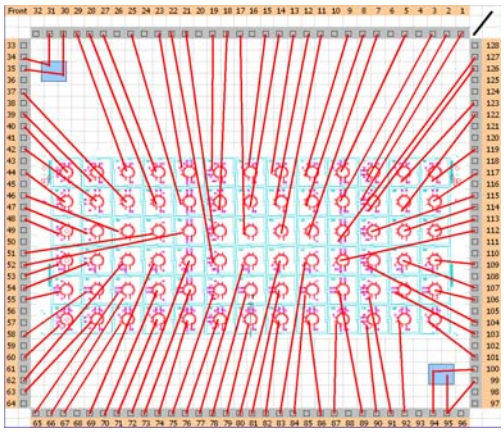

Figure 1. Picture of LWIR half wafer containing 75 (photodiodes

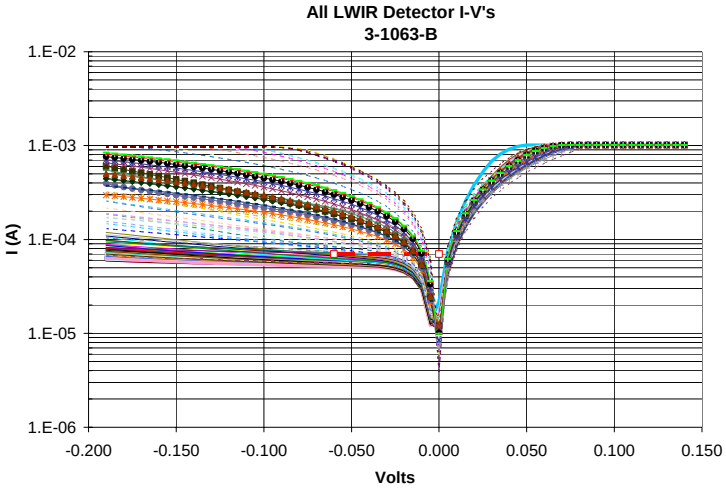

Figure 2. I-V curves for 69 photodiodes from an LWIR half-wafer

2.2 Single photodiode I-V, Quantum Efficiency, Spectral Response and Noise

Each candidate detector selected from the half-wafer I-V measurement is mounted into a leadless chip carrier and characterized for its I-V characteristics, noise under dark and illuminated conditions, spectral response and quantum efficiency performance at the specified operating temperature. Noise is measured at the nominal flux at which the photodiode will operate within the CrIS instrument.

A commercial Fourier transform infrared spectrometer is used to obtain the spectral response at 81K for all the LWIR photodiodes. All measurements are made at the temperature and bias at which the photodiodes will operate within the CrIS instrument. For the LWIR photodiodes, absolute quantum efficiency is measured at λ = 10.6 μm using a narrow band filter. Narrow band filters centered at λ = 7.4 μm and λ = 4.0 μm are used for the MWIR and SWIR photodiodes quantum efficiency measurements. The quantum efficiency and spectral cut-off are traceable to NIST. The quantum efficiency using a narrow band filter is combined with the spectral response curve to obtain the quantum efficiency versus wavelength curve as displayed in Figure 3 for a representative LWIR photodiode. Quantum efficiency as a function of wavelength is a principal specification that has to be met for a photodiode to be utilized in the CrIS instrument. The specification quantum efficiency is also displayed in Figure 3 as a dashed red line. Figure 4 is a two dimensional spot scan of a LWIR photodiode. The set-up used in the spot scan measurement is the same as that used for the narrow band filter quantum efficiency measurement. The incident radiation from a blackbody source passes through an aperture and a narrow band filter centered at λ = 10.5 μm. The incident radiation is focused onto the detector by an f/1.6 lens. The spot size is calculated to be ~ 70 μm for the blackbody aperture size, system configuration and lens utilized. Response measurements were obtained in 100 μm steps. The full width half maximum (FWHM) is measured at ~ 820 μm in Figure 4. The uncertainty in the FWHM is impacted by the large spot size.

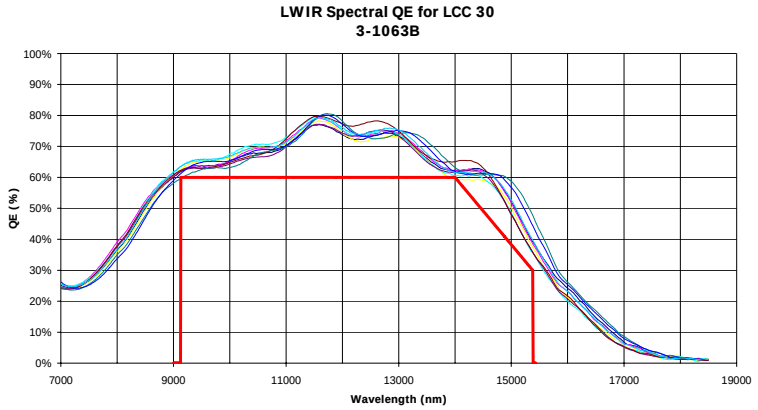

Figure 3. Quantum efficiency versus wavelength for a LWIR [λ_c(81 K) ~ 1A.B μm] photodiode

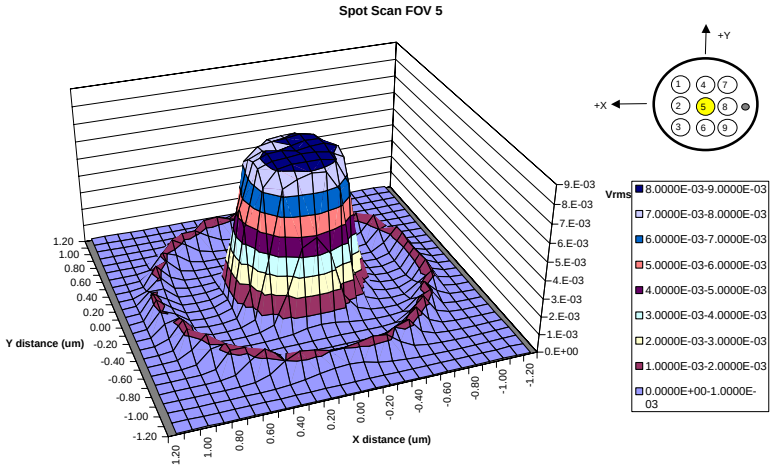

Figure 4. 2-D spot scan of a LWIR [λ_c(81 K) ~ 10.6 μm] photodiode at 81 K

I-V and noise is measured[4,5] for all nine photodiodes in each LCC at the operating temperature, i.e. LWIR are measured at 81 K, whereas MWIR and SWIR photodiodes are measured at 98 K. Figures 5a and 5b are the I-V and noise spectral density curves in the dark from an LCC containing LWIR photodiodes. The dark current at 60 mV reverse bias is ~ 5 x 10^{-5} A. This translates into a white noise ~ 4 x 10^{-12} A/Hz$^{1/2}$. Some of the photodiodes are at the calculated white noise level by ~ 10 kHz. These are the photodiodes that are selected for placement in the FPAA. Similar measurements and calculations are made for the MWIR photodiodes. SWIR photodiodes at 98 K have calculated white noise values in the low 10^{-15} A/Hz$^{1/2}$ range. This noise level is impossible to measure consistently and accurately using the noise measurement station[4] and commercial amplifiers such as the Ithaco 1211 that are run at room temperature. Figures 6a and 6b are similar curves for the same nine photodiodes while illuminated, the flux being the instrument nominal flux condition Φ = 3.5 x 10^{17} ph/cm^2/s for the LWIR color. The total current (dark + photocurrent) for the LWIR photodiodes is ~ 2.7 x 10^{-4} A, translating into a white noise of ~ 9 x 10-12 A/Hz$^{1/2}$.

There exists a one-to-one correlation between spectral wavelength and noise frequency in a Fourier transform infrared spectrometer. In the CrIS instrument for example, λ = 15.38 μm corresponds to f = 6.5 kHz, λ = 14.01 μm corresponds to f = 7.1 kHz and λ = 10.5 μm corresponds to f = 9.5 kHz. Therefore, when computing D* for a photodiode, the quantum efficiency and hence responsivity at any wavelength λ_i needs to be calculated using the corresponding frequency f_i. LWIR photodiodes that are at or near the calculated white noise level at 6.5 kHz are selected for placement in the FPAA. This insures that within the 9.ab μm to 15.38 μm spectral range that the LWIR FPAA covers, photocurrent is the dominant noise source. LCCs containing MWIR and SWIR photodiodes are measured at $\Phi = 6.2 \times 10^{16}$ ph/cm^2/s and $\Phi = 1.8 \times 10^{15}$ ph/cm^2/s respectively. Similar procedures are followed for the selection of MWIR and SWIR photodiodes prior to their selection for placement into FPAAs.

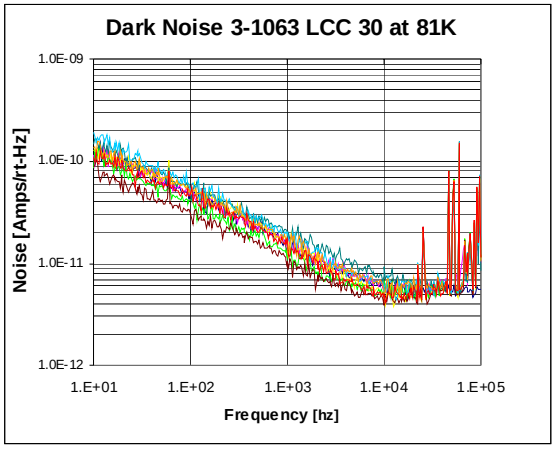

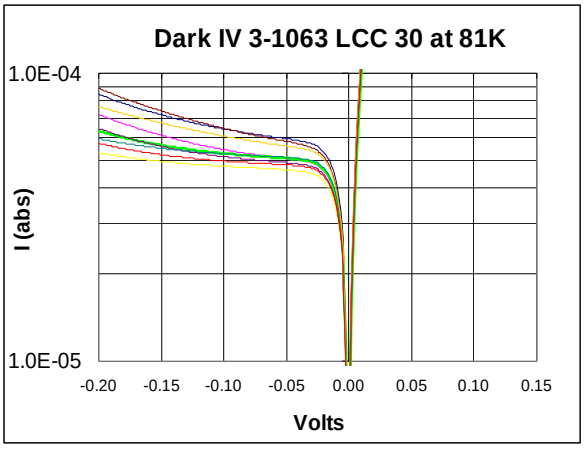

Figure 5a and 5b. Dark noise and I-V measurements for nine LWIR photodiodes at 81 K.

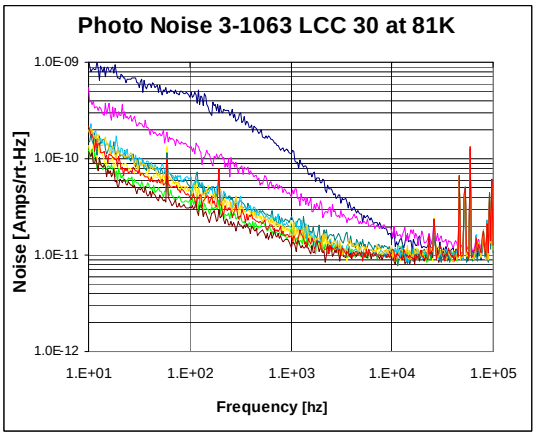

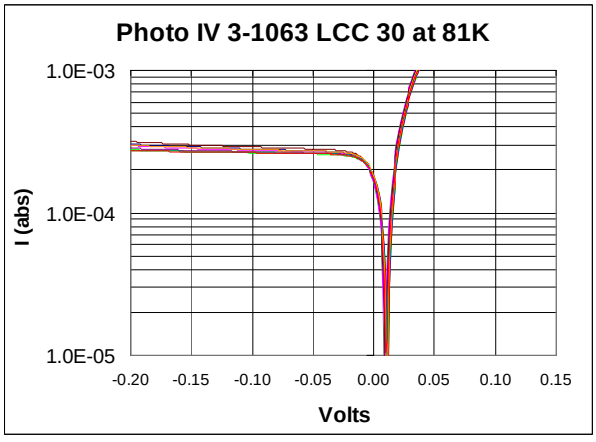

Figure 6a and 6b. Illuminated ($\Phi = 3.5 \times 10^{17}$ ph/cm^2/s) noise and I-V measurements at 81 K for same nine photodiodes as in Figures 5 and 5b

3.0 FPAA Module

The Flight configuration for the CrIS Detector Preamplifier Module (DPM)[6] consists of three spectrally separate (SWIR, MWIR and LWIR) FPAAs, three (SWIR, MWIR and LWIR) signal flex cable assemblies, a warm signal flex cable, vacuum bulk head assembly, and the DPM warm electronics circuit card assemblies (CCAs) as shown in figure 7. The photodiodes are operated at reverse bias for the LWIR and MWIR, and at or near zero bias, for the SWIR coupled to a differential J-FET buffered, resistive feedback, transimpedance amplifier (RTIA). The RTIA provides the necessary gain for the circuit, and the J-FET differential buffers provide low noise, current to voltage conversion at constant output impedance. Custom preamplifiers for each spectral band have been designed. Each FPAA contains a 3 x 3 array of nine 850 μm diameter photovoltaic detectors, each driving its own RTIA, with their associated cold electronics, detector optics assembly, and two flex cable assemblies with interface connectors. The FPAAs (detector arrays, detector optics assemblies, JFET buffer and feedback resistor portions of the transimpedance preamplifier, and flex cable assemblies) are cooled to cryogenic temperatures by the detector cooler module in their final configuration. The cryogenic portions of the DPM (FPAAs, and Signal Flex Cable Assemblies) mate to the ambient temperature portions of the DPM (warm signal flex cable assembly and the ambient temperature portions of the transimpedance amplifier, mounted within the CCAs) through the vacuum bulk head assembly mounted on the detector cooler assembly housing.

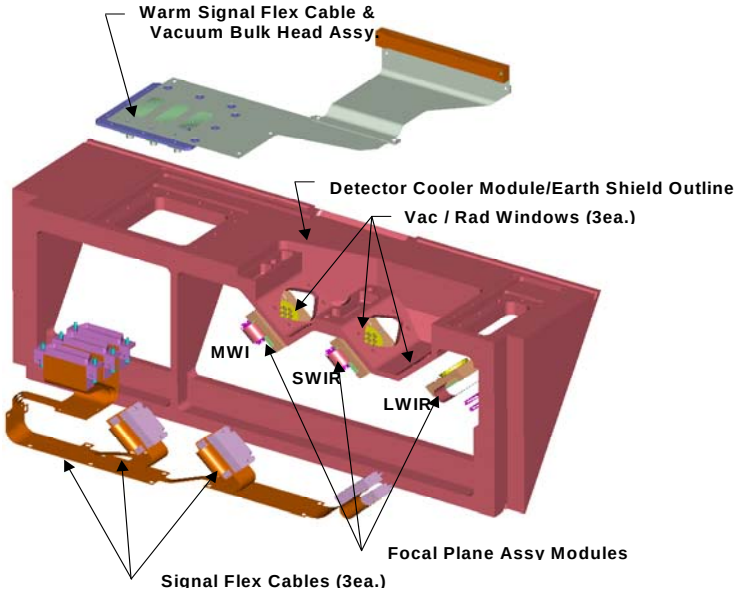

Figure 7. CrIS detector Preamplifier Module (Warm electronics CCAs not shown)

Quantum efficiency versus wavelength and noise spectral density under dark and illuminated conditions are used to determine the nine photodiodes of each color that are integrated in the FPAA. These detectors are placed in a 3 x 3 grid array on the base of the module with a placement accuracy of +/- 2μm from FOV to FOV. Placement of the photodiodes into the sapphire carrier is a critical step in the assembly of the FPAA. Due to the brittle nature of Mercury Cadmium Telluride (HgCdTe), the mounting process can cause damage to the photodiode, decreasing its performance[7]. Careful procedures are followed to prevent degradation in performance for the LCC demounting to FPAA mounting and assembly sequence. A picture of an assembled FPAA is shown in figure 8. Since the photodiodes are backside illuminated, the metal pad that connects the 7 μm diameter p-type implants together to form a single 850 μm diameter lateral collection detector can be clearly seen in the picture. Also seen are the discrete components (JFETs, resistors etc.) that constitute the preamplifier module.

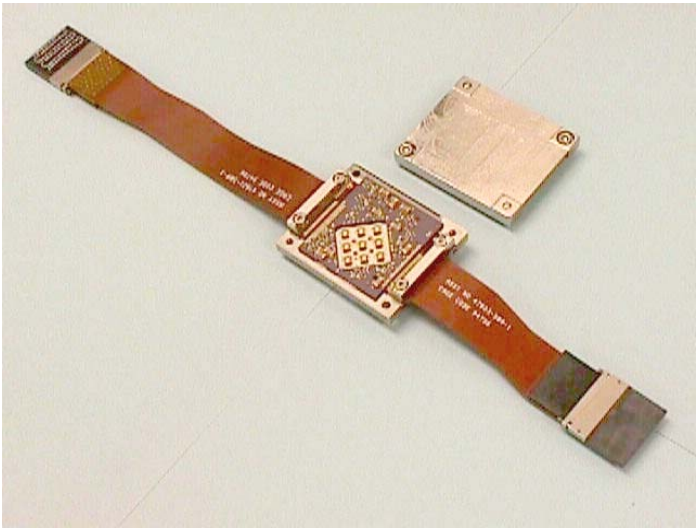

Figure 8. Assembled CrIS LWIR FPAA module

3.1 LWIR FPAA Data

Nine candidate LWIR photodiodes are mounted on the sapphire base and incorporated into the LWIR FPAA along with the preamplifier, cables etc. as shown in figure 8. The LWIR FPAA is cooled to 81 K and the photodiodes are held at 60 mV reverse bias during subsequent responsivity and noise measurements. The reason for holding the photodiodes in reverse bias is two-fold. The impedance of large λ_c(98 K) ~ 9 μm, and λ_c(81 K) ~ 15.5 μm photodiodes is quite low at zero bias. A pre-amplifier interfacing with a low impedance detector results in high noise in the pre-amplifier. Also, the injection efficiency is depressed, rendering it impossible to extract the photocurrent efficiently. Consequently, the external quantum efficiency is low. Operating the detector in reverse bias can increase the detector dynamic impedance by two orders of magnitude, resulting in the external quantum efficiency rising to the value of the internal quantum efficiency. However, operating photodiodes in reverse bias results in the photodiodes having excess low frequency or 1/f noise. Therefore, a balance is struck between increasing 1/f noise, pre-amplifier noise and injection efficiency to maximize performance for the entire photodiode, pre-amplifier train.

Noise measurements at the nominal operating flux of $\Phi = 3.5 \times 10^{17}$ photons·cm^{-2}·s^{-1} are made for all the photodiodes in the FPAA. These flux values are achieved using an Electro-Optical Industries (EOI) Black Body mounted external to the dewar. The dewar flux is calibrated using a detector with known quantum efficiency. The noise spectral density for all nine channels is plotted in figure 9. The CCA is AC coupled for this measurement, which explains the 300 Hz roll on of the high pass filter. For the LWIR FPAA, the electrical band of interest is 6.5 - 10.95 kHz. To obtain maximum performance, the photodiode noise needs to be photon noise dominated within the frequency band of interest. The gain of the pre-amplifier is designed to be maintained constant within the frequency band of interest. As stated previously, there is a one-to-one correspondence between response at a particular wavelength λ_i and noise at frequency f_i. To calculate D* at any wavelength, the quantum efficiency at any wavelength $\eta(\lambda)$, is ratioed to the noise corresponding to that particular wavelength. The other parameters listed in the D* equation 1 below are then input to calculate D* as a function of wavelength, $D^*(\lambda)$. Figure 10 is a plot of D* versus λ for all the nine photodiodes in the LWIR FPAA. The requirement at λ = 14.01 μm is D* > 4.0 x 10^{10} cm $Hz^{1/2}$/W. All the photodiodes exceed the D* requirement.

$$D^*(\lambda) = \frac{q\lambda A_{\det}^{\frac{1}{2}}\eta(\lambda)}{hci_n(\lambda)} \qquad (1)$$

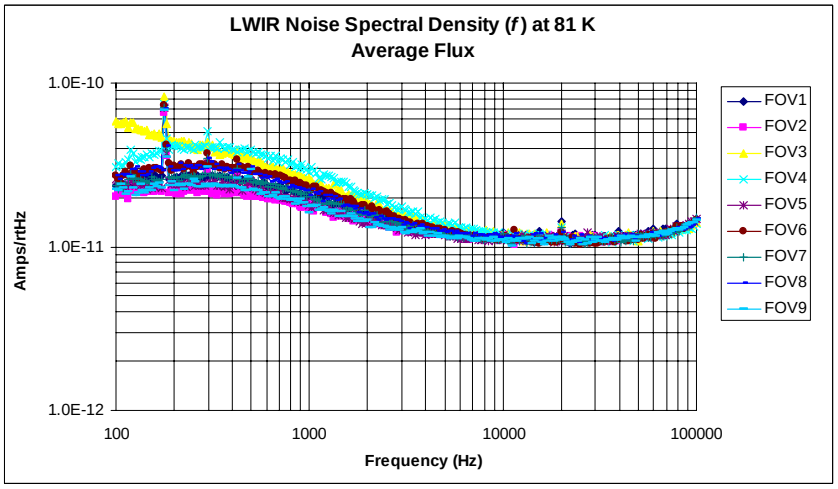

Figure 9. Noise spectral density for all nine photodiodes in the LWIR FPAA, measured at 81 K, V_d = -60 mV and $\Phi = 3.5 \times 10^{17}$ photons·cm^{-2}·s^{-1}

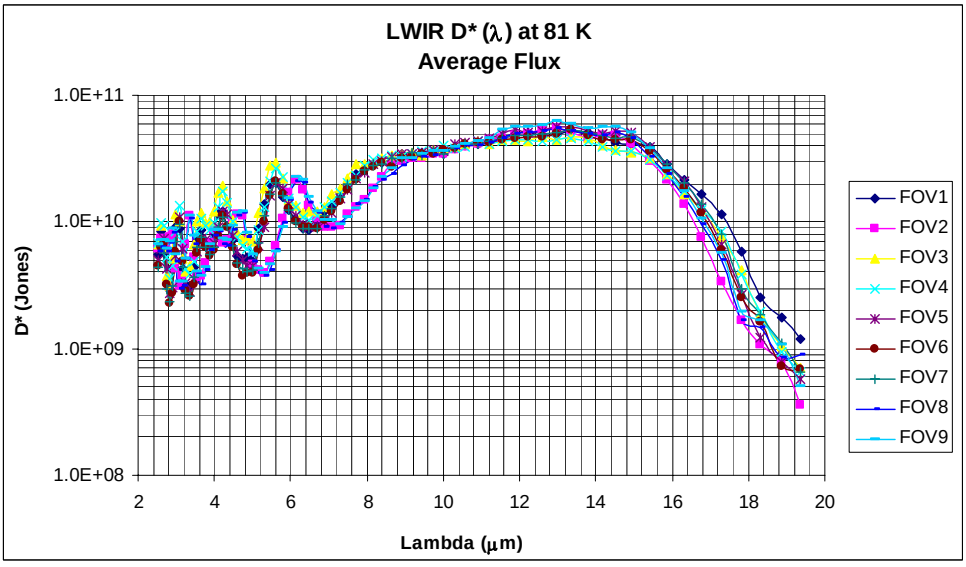

Figure 10. LWIR Spectral D* at 81 K and nominal flux $\Phi = 3.5 \times 10^{17}$ photons·cm^{-2}·s^{-1}

3.2 LWIR FPAA Baking Data

The NPOESS satellite, CrIS instrument and consequently the three FPAAs are subject to various environmental conditions, one of which is a 65 C bake for 21 days. Therefore, an LWIR Qualification FPAA was assembled to observe the effects of baking on FPAA performance. The reason the LWIR FPAA was chosen was that baking at elevated temperatures should be most stressing to the LWIR photodiodes. Effects should be smaller on the MWIR and SWIR photodiodes. Table A is the relative change in dark current and noise with respect to the initial FPAA measurement, as a function of bake time, for the nine photodiodes. The bake temperature was 70° C. As can be seen from the figure, there was no change in photodiode performance as a function of baking out to 2800 hours. Any variations observed are a consequence of measurement variability.

FOV	Pedigree	Relative Change upto 14 day Bake			Relative Change upto 31 day Bake			Relative Change upto 60 day Bake			Relative Change Pre & Post Bake		
		Id	Rd	Noise	Id	Rd	Noise	Id	Rd	Noise	Id	Rd	Noise
1	Lot 5 B	0.98	0.92	0.99	0.96	1.02	1.08	0.96	1.11	1.15	0.96	0.89	1.02
2	Lot 5 B	0.83	0.76	0.81	0.78	0.75	0.79	0.74	0.78	0.78	0.75	0.70	0.97
3	Lot 5 B	0.80	0.76	0.67	0.75	0.75	0.62	0.70	0.70	0.64	0.71	0.58	1.03
4	Lot 5 B	0.99	1.00	0.96	1.00	1.10	0.87	1.02	1.10	0.92	1.04	1.17	1.01
5	Lot 5 B	0.83	0.70	0.90	0.79	0.64	0.78	0.77	0.60	0.87	0.78	0.58	1.01
6	Lot 5 A	0.97	1.30	1.41	1.02	1.46	1.41	1.05	1.54	1.58	1.04	0.86	1.03
7	Lot 5 B	1.57	2.77	0.83	1.49	2.53	0.87	1.41	2.57	1.01	1.43	2.31	1.16
8	Lot 5 A	1.00	1.02	1.29	1.01	0.93	1.48	1.00	0.97	1.53	0.98	0.93	1.01
9	Lot 5 A	1.03	1.35	1.25	1.06	1.44	1.07	1.06	1.50	1.31	1.05	0.62	1.05

Table A. Relative change in dark current, dynamic resistance and noise for all LWIR FPAA FOVs

3.3 MWIR FPAA Data

The MWIR FPAA is cooled to 98 K and the photodiodes are also held at 60 mV reverse bias as in the LWIR FPAA case. Noise measurements are made at the nominal $\Phi = 6.2 \times 10^{16}$ photons·cm^{-2}·s^{-1}. The electrical band of interest is 12.1-17.5 kHz, corresponding to wavelengths $\lambda = 8.26$ μm down to $\lambda = 5.ab$ μm. Spectral D* as a function of wavelength is plotted in Figure 11. The average D* at 8.26 μm was 1.00×10^{11} +/- 8.0×10^{9} cm-Hz$^{1/2}$/W, exceeding the specification D* = 7.5×10^{10} cm-Hz$^{1/2}$/W.

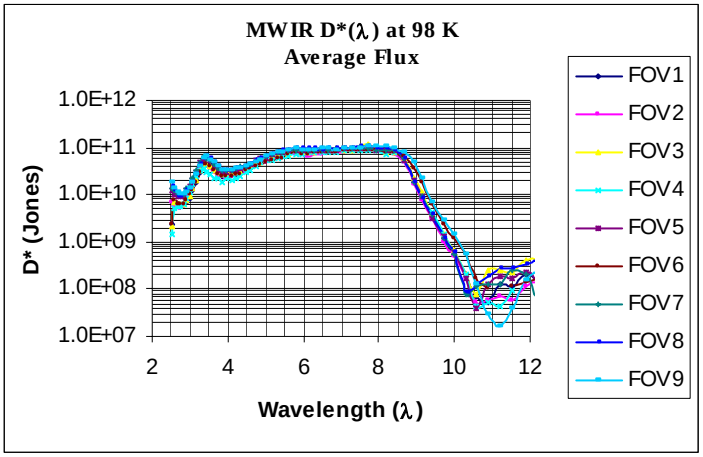

Figure 11. MWIR Spectral D* at 98 K and nominal flux $\Phi = 6.2 \times 10^{16}$ photons·cm^{-2}·s^{-1}

3.4 SWIR FPAA Data

The SWIR FPAA is cooled to 98 K and the detectors are held at -5 mV reverse bias. SWIR photodiode impedance at 98 K near zero bias is in the ~ XX ohms range. Therefore the photodiodes do not have to be held in reverse bias to obtain high injection efficiency or low noise in the pre-amplifier. Noise measurements are made at the nominal Φ = X.Y x 10^{15} photons·cm^{-2}·s^{-1}. The electrical band of interest is 21.5-25.5 kHz, corresponding to wavelengths λ = 4.64 μm down to λ = 3.92 μm. Spectral D* as a function of wavelength is plotted in Figure 12. The average D* at 4.64 μm is 3.1 x 10^{11} +/- 7.4 x 10^{9} cm-Hz$^{1/2}$/W, exceeding the specification D* = 3.0 x 10^{11} cm-Hz$^{1/2}$/W and close to the BLIP D* of 4.2 x 10^{11} cm-Hz$^{1/2}$/W. The BLIP D* is calculated using a quantum efficiency = 1.

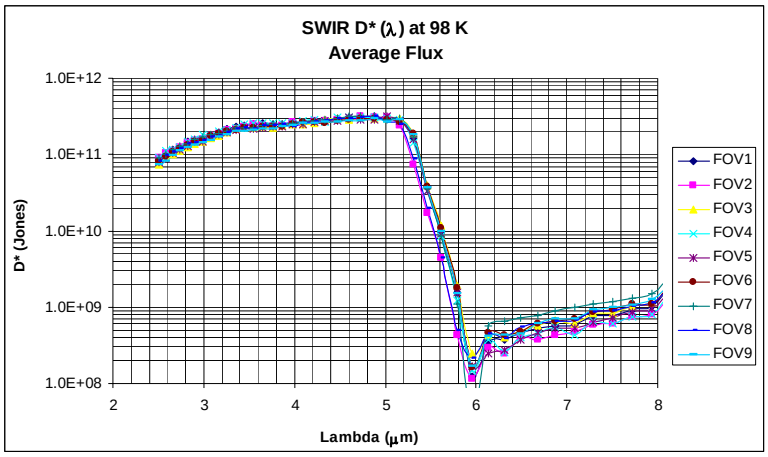

Figure 12. SWIR Spectral D* at 98 K and nominal flux Φ = X.Y x 10^{15} photons·cm^{-2}·s^{-1}

5.0 SUMMARY

The appropriate bandgap n-type $Hg_{1-x}Cd_xTe$ was grown on lattice-matched CdZnTe. 850-μm-diameter photodiodes were manufactured using a Lateral Collection Diode (LCD) architecture. Custom pre-amplifiers are separately designed to interface with the large LWIR and MWIR low impedance photodiodes and with SWIR photodiodes at frequencies up to 25.5 kHz. Pre-amplifier gain is maintained constant within the electrical band of interest for each color. The LWIR, MWIR and SWIR photodiodes are operated at 81 K, 98 K and 98 K respectively. Performance goals are D* = 5.0 x 10^{10} cm-Hz$^{1/2}$/W at 14.0 μm, 9.3 x 10^{10} cm-Hz$^{1/2}$/W at 8.0 μm and 3.0 x 10^{11} cm-Hz$^{1/2}$/W at 4.64 μm. Measured mean values for the nine photodiodes in each of the LWIR, MWIR and SWIR FPAAs are D* = 5.3 x 10^{10} cm-Hz$^{1/2}$/W at 14.01μm, 1.0 x 10^{11} cm-Hz$^{1/2}$/W at 8.26 μm and 3.1 x 10^{11} cm-Hz$^{1/2}$/W at 4.64 μm. These compare favorably with the BLIP calculated at the nominal flux condition are D* = 8.36 x 10^{10} cm Hz$^{1/2}$/W at 14.01 μm, 1.4 x 10^{11} cm-Hz$^{1/2}$/W at 8.26 μm and 4.1 x 10^{11} cm-Hz$^{1/2}$/W at 4.64 μm.

6.0 REFERENCES

1. A.I. D'Souza, L.C. Dawson, E.J. Anderson, A.D. Markum, W.E. Tennant, L.O. Bubulac, M. Zandian, J.G. Pasko, W.V. McLevige, D.D. Edwall, *J. Electron. Mater.* 26, 656 (1997).
2. H. Holloway, *J. Appl. Phys.* , **49**, 4264 (1978)
3. P.S. Wijewarnasuriya, M. Zandian, D.B. Young, J. Waldrop, D.D. Edwall, W.V. McLevige, J. Arias, A.I. D'Souza, *J. Elecctron. Mater.* **28**, 649 (1999).
4. A.I. D'Souza, M.G. Stapelbroek, P.N. Dolan, P.S. Wijewarnasuriya, R.E. DeWames, D.S. Smith, J.C. Ehlert, J. of Electronic Materials, 32, 633 (2003).

5. A.I. D'Souza, M.G. Stapelbroek, P.S. Wijewarnasuriya, R.E. DeWames, D.S. Smith, J.C. Ehlert, SPIE Proceedings Vol. 4820, pg. 389, Intl. Sym. on Optical Science and Tech., 7 - 11 July 2002, Seattle, WA.
6. A.I. D'Souza, L.C. Dawson, S. Marsh, R. Willis, P.S. Wijewarnasuriya, R.E. DeWames, J.M. Arias, J. Bajaj, G. Hildebrandt, F.E. Moore, SPIE Proc. Vol. 4369, p. 157.
7. A.I. D'Souza et al, 2004 II-VI workshop extended abstracts.